

# We are IntechOpen, the world's leading publisher of Open Access books Built by scientists, for scientists

6,900

Open access books available

185,000

International authors and editors

200M

Downloads

Our authors are among the

154

Countries delivered to

TOP 1%

most cited scientists

12.2%

Contributors from top 500 universities



WEB OF SCIENCE™

Selection of our books indexed in the Book Citation Index  
in Web of Science™ Core Collection (BKCI)

Interested in publishing with us?  
Contact [book.department@intechopen.com](mailto:book.department@intechopen.com)

Numbers displayed above are based on latest data collected.  
For more information visit [www.intechopen.com](http://www.intechopen.com)



---

# Optical Phase-Conjugation of Picosecond Four-Wave Mixing Signals in SOAs

---

Narottam Das, Hitoshi Kawaguchi and Mohammad Razaghi

Additional information is available at the end of the chapter

<http://dx.doi.org/10.5772/51390>

---

## 1. Introduction

The application of four-wave mixing (FWM) in semiconductor optical amplifiers (SOAs) has been widely demonstrated to all-optical devices, such as wavelength converters (Vahala *et al.*, 1996; Nettet *et al.*, 1998), optical samplers (Kawaguchi & Inoue, 1998), optical multiplexers/ demultiplexers (Kawanishi *et al.*, 1997; Uchiyama *et al.*, 1998; Tomkos *et al.*, 1999; Buxens *et al.*, 2000; Set *et al.*, 1998), and optical phase conjugators (Dijaili *et al.*, 1990; Kikuchi & Matsumura, 1998; Marcenac *et al.*, 1998; Corchia *et al.*, 1999; Tatham *et al.*, 1993; Ducellier *et al.*, 1996), which are expected to be used in future optical communication systems. Kikuchi & Matsumura have demonstrated the transmission of 2-ps optical pulses at 1.55  $\mu\text{m}$  over 40 km of standard fiber by employing midspan optical phase conjugation in SOAs (Kikuchi & Matsumura, 1998). An ideal phase conjugator must reverse the chirp of optical pulses while maintaining the pulse waveform. Kikuchi & Matsumura (Kikuchi & Matsumura, 1998) have shown that the second-order dispersion is entirely compensated by the optical phase-conjugation obtained using SOAs with a continuous wave (cw) input pump wave. All-optical demultiplexing (DEMUX), based on FWM in SOAs, was also demonstrated. When a single pulse of a time-multiplexed signal train (as probe pulses) and a pump pulse are injected simultaneously into an SOA, the gain and refractive index in the SOA are modulated, and an FWM signal pulse is created by the modulations. Thus, we can obtain a demultiplexed signal as the FWM signal by Das *et al.*, (Das *et al.*, 2000). All-optical DEMUX has been experimentally demonstrated up to 200 Gbit/s by Kawanishi *et al.*, (Kawanishi *et al.*, 1997). Many research reports have been published recently on the theoretical investigation of the characteristics of FWM for short optical pulses in SOAs. Tang and Shore (Tang & Shore, 1999) theoretically examined the dynamical chirping of mixing pulses and showed that all mixing pulses have negative pulse chirp except in the far edges of trailing pulses, indicating that pulse spectra are primarily red-shifted. The demultiplexed signals obtained as FWM signals may still have optical phase-conjugate characteristics,

although they may include waveform distortion and additional chirp. If the demultiplexed signal obtained as the FWM signal has optical phase-conjugate characteristics, the demultiplexed signal can be compressed using a dispersive medium. However, such optical phase-conjugate characteristics of FWM signals have not yet been reported to the best of author's knowledge. Another advantage of FWM with short duration optical pump pulses is the high conversion efficiency. In conventional systems, the FWM conversion efficiency in an SOA is limited due to gain saturation. However, high FWM conversion efficiency can be achieved with short duration optical pump and probe pulses as it is possible to reduce gain saturation and hence increase FWM conversion efficiency in an SOA by applying strong pump intensity (Shtaif & Eisenstein, 1995; Shtaif *et al.*, 1995; Kawaguchi & Inoue, 1996a; Kawaguchi & Inoue, 1996b).

In this chapter, we present the detail numerical simulation results of optical phase-conjugate characteristics of picosecond FWM signal pulses generated in SOAs using the FD-BMP (Das *et al.*, 2000; Razaghi *et al.*, 2009). These simulations are based on the nonlinear propagation equation considering the group velocity dispersion, self-phase modulation (SPM), and two-photon absorption (TPA), with the dependencies on the carrier depletion (CD), carrier heating (CH), spectral-hole burning (SHB), and their dispersions, including the recovery times in SOAs (Hong *et al.*, 1996). The main purpose of our simulations is to provide answers to the following questions: 1) how is the nature of the optical phase-conjugate maintained for a short FWM signal pulse? 2) how does the chirp observed in the FWM signals affect the nature of the optical phase-conjugate? For this reason, we have analyzed the system in which the Fourier transform-limited Gaussian optical pulse is linearly chirped by transmission through a fiber (Fiber I) and then injected into an SOA as a probe pulse, together with a pump pulse that has a 1 ~ 10 ps pulsewidth. The FWM signal is generated by the mixing of the pump pulse and the probe pulse, and is selected by an optical narrow band-pass filter. The FWM signal is then transmitted through another fiber (Fiber II) that has the same group velocity dispersion (GVD) as Fiber I and an appropriate length. The simulations are based on the nonlinear propagation equation considering the GVD, SPM, and TPA, with dependencies on CD, CH, SHB, and dispersion of those properties (Das *et al.*, 2000; Hong *et al.*, 1996).

The FD-BPM is useful to obtain the propagation characteristics of single pulse or multi-pulses using the modified nonlinear Schrödinger equation (MNLSE) (Hong *et al.*, 1996 & Das *et al.*, 2000), simply by changing only the combination of input optical pulses. These are: (1) single pulse propagation (Das *et al.*, 2008), (2) FWM characteristics using two input pulses (Das *et al.*, 2000), (3) optical DENUX using several input pulses (Das *et al.*, 2001), (4) optical phase-conjugation using two input pulses with chirp (Das *et al.*, 2001) and (5) optimum time-delayed FWM characteristics between the two input pump and probe pulses (Das *et al.*, 2007).

## 2. Analytical model

In this section, we briefly discuss the important nonlinear effects in SOAs, mathematical formulation of modified nonlinear Schrödinger equation (MNLSE), finite-difference beam

propagation method (FD-BPM) that is used in the simulation, and nonlinear propagation characteristics of solitary optical pulses in SOAs.

## 2.1. Important nonlinear effects in SOAs

There are several types of “nonlinear effects” occurs in SOAs. Among them, the important four types of “nonlinear effects” are shown in Fig. 1. These are namely: (i) spectral hole-burning (SHB), (ii) carrier heating (CH), (iii) carrier depletion (CD) and (iv) two-photon absorption (TPA).

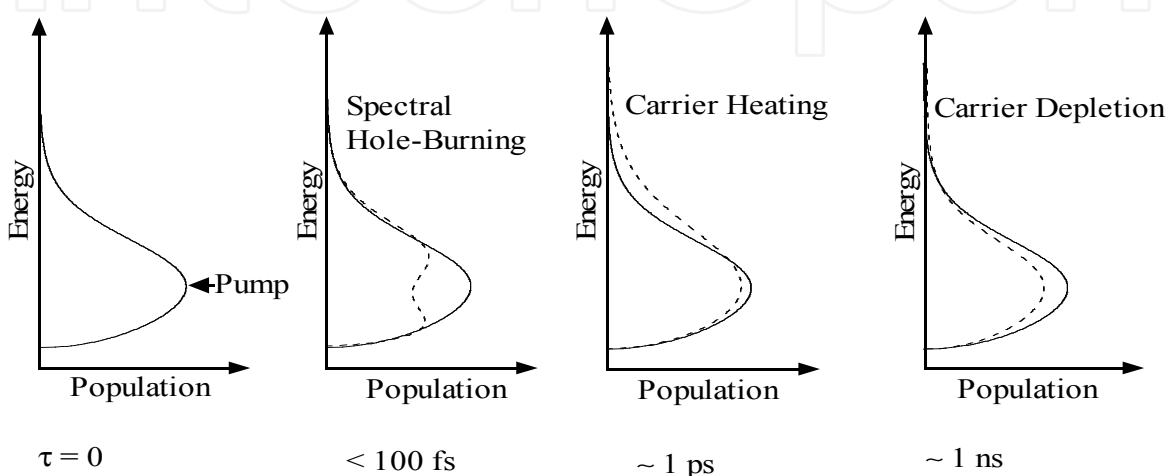


**Figure 1.** The important nonlinear effects in SOAs: (i) spectral hole-burning (SHB) with a life time of less than 100 fs (i.e.,  $< 100$  fs), (ii) carrier heating (CH) with a life time of  $\sim 1$  ps, (iii) carrier depletion (CD) with a life time is  $\sim 1$  ns and (iv) two-photon absorption (TPA).

Figure 1 shows the time-development of the population density in the conduction band after excitation (Das, 2000). The arrow (pump) shown in Fig. 1 is the excitation laser energy. When the life time is less than 100 fs (i.e.,  $< 100$  fs), the SHB effect is dominant. The SHB occurs when a narrow-band strong pump beam excites the SOA, which has an inhomogeneous broadening. The SHB arises due to the finite value of intraband carrier-carrier scattering time ( $\sim 50 - 100$  fs), which sets the time scale on which a quasi-equilibrium Fermi distribution is established among the carriers in a band. After the life time  $\sim 1$  ps, the SHB effect is relaxed and the CH effect becomes dominant. The process tends to increase the temperature of the carriers beyond the lattice’s temperature. The main causes of heating the carriers are (1) the stimulated emission, since it involves the removal of “cold” carriers close to the band edge and (2) the free-carrier absorption, which transfers carriers to high energies within the bands. The “hot”-carriers relax to the lattice temperature through the emission of optical phonons with a relaxation time of  $\sim 0.5 - 1$  ps. The effect of CD remains for about 1 ns. The stimulated electron-hole recombination depletes the carriers, thus reducing the optical gain. The band-to-band relaxation also causes CD, with a relaxation time of  $\sim 0.2 - 1$  ns. For ultrashort optical pumping, the TPA effect also becomes important. An atom makes a transition from its ground state to the excited state by the simultaneous absorption of two laser photons. All these nonlinear effects (mechanisms) are taken into account in the

modeling/ simulation and the mathematical formulation of modified nonlinear Schrödinger equation (MNLSE).

## 2.2. Mathematical Formulation of Modified Nonlinear Schrödinger Equation (MNLSE)

In this subsection, we will briefly explain the theoretical analysis of short optical pulses propagation in SOAs. We start from Maxwell's equations (Agrawal, 1995; Yariv, 1991; Sauter, 1996) and reach the propagation equation of short optical pulses in SOAs, which are governed by the wave equation (Agrawal & Olsson, 1989) in the frequency domain.

$$\nabla^2 \bar{E}(x, y, z, \omega) + \frac{\epsilon_r}{c^2} \omega^2 \bar{E}(x, y, z, \omega) = 0 \quad (1)$$

where,  $\bar{E}(x, y, z, \omega)$  is the electromagnetic field of the pulse in the frequency domain,  $c$  is the velocity of light in vacuum and  $\epsilon_r$  is the nonlinear dielectric constant which is dependent on the electric field in a complex form. By slowly varying the envelope approximation and integrating the transverse dimensions we arrive at the pulse propagation equation in SOAs (Agrawal & Olsson, 1989; Dienes *et al.*, 1996).

$$\frac{\partial V(\omega, z)}{\partial z} = -i \left\{ \frac{\omega}{c} [1 + \chi_m(\omega) + \Gamma \tilde{\chi}(\omega, N)]^{1/2} - \beta_0 \right\} V(\omega, z) \quad (2)$$

where,  $V(\omega, z)$  is the Fourier-transform of  $V(t, z)$  representing pulse envelope,  $\chi_m(\omega)$  is the background (mode and material) susceptibility,  $\tilde{\chi}(\omega)$  is the complex susceptibility which represents the contribution of the active medium,  $N$  is the effective population density,  $\beta_0$  is the propagation constant. The quantity  $\Gamma$  represents the overlap/ confinement factor of the transverse field distribution of the signal with the active region as defined in (Agrawal & Olsson, 1989).

Using mathematical manipulations (Sauter, 1996; Dienes *et al.*, 1996), including the real part of the instantaneous nonlinear Kerr effect as a single nonlinear index  $n_2$  and by adding the TPA term we obtain the MNLSE for the phenomenological model of semiconductor laser and amplifiers (Hong *et al.*, 1996). The following MNLSE (Hong *et al.*, 1996; Das *et al.*, 2000) is used for the simulation of FWM characteristics and optical phase-conjugation characteristics with input pump and probe pulses in SOAs.

$$\left[ \frac{\partial}{\partial z} - \frac{i}{2} \beta_2 \frac{\partial^2}{\partial \tau^2} + \frac{\gamma}{2} + \left( \frac{\gamma_{2p}}{2} + i b_2 \right) |V(\tau, z)|^2 \right] V(\tau, z) = \left\{ \frac{1}{2} g_N(\tau) \left[ \frac{1}{f(\tau)} + i \alpha_N \right] + \frac{1}{2} \Delta g_T(\tau) (1 + i \alpha_T) - i \frac{1}{2} \frac{\partial g(\tau, \omega)}{\partial \omega} \bigg|_{\omega_0} \frac{\partial}{\partial \tau} - \frac{1}{4} \frac{\partial^2 g(\tau, \omega)}{\partial \omega^2} \bigg|_{\omega_0} \frac{\partial^2}{\partial \tau^2} \right\} V(\tau, z) \quad (3)$$

Here, we introduce the frame of local time  $\tau (= t - z/v_g)$ , which propagates with a group velocity  $v_g$  at the center frequency of an optical pulse. A slowly varying envelope

approximation is used in (3), where the temporal variation of the complex envelope function is very slow compared with the cycle of the optical field. In (3),  $V(\tau, z)$  is the time domain complex envelope function of an optical pulse,  $|V(\tau, z)|^2$  represents the corresponding optical pulse power, and  $\beta_2$  is the GVD.  $\gamma$  is the linear loss,  $\gamma_{2p}$  is the TPA coefficient,  $b_2 (= \omega_0 n_2 / cA)$  is the instantaneous SPM term due to the instantaneous nonlinear Kerr effect  $n_2$ ,  $\omega_0 (= 2\pi f_0)$  is the center angular frequency of the pulse,  $c$  is the velocity of light in vacuum,  $A (= wd/\Gamma)$  is the effective area ( $d$  and  $w$  are the thickness and width of the active region, respectively and  $\Gamma$  is the confinement factor) of the active region.

The saturation of the gain due to the CD is given by (Hong *et al.*, 1996)

$$g_N(\tau) = g_0 \exp\left(-\frac{1}{W_s} \int_{-\infty}^{\tau} e^{-s/\tau_s} |V(s)|^2 ds\right) \quad (4)$$

where,  $g_N(\tau)$  is the saturated gain due to CD,  $g_0$  is the linear gain,  $W_s$  is the saturation energy,  $\tau_s$  is the carrier lifetime.

The SHB function  $f(\tau)$  is given by (Hong *et al.*, 1996)

$$f(\tau) = 1 + \frac{1}{\tau_{shb} P_{shb}} \int_{-\infty}^{+\infty} u(s) e^{-s/\tau_{shb}} |V(\tau - s)|^2 ds \quad (5)$$

where,  $f(\tau)$  is the SHB function,  $P_{shb}$  is the SHB saturation power,  $\tau_{shb}$  is the SHB relaxation time, and  $\alpha_N$  and  $\alpha_T$  are the line width enhancement factor associated with the gain changes due to the CD and CH.

The resulting gain change due to the CH and TPA is given by (Hong *et al.*, 1996)

$$\begin{aligned} \Delta g_T(\tau) = & -h_1 \int_{-\infty}^{+\infty} u(s) e^{-s/\tau_{ch}} (1 - e^{-s/\tau_{shb}}) |V(\tau - s)|^2 ds \\ & - h_2 \int_{-\infty}^{+\infty} u(s) e^{-s/\tau_{ch}} (1 - e^{-s/\tau_{shb}}) |V(\tau - s)|^4 ds \end{aligned} \quad (6)$$

where,  $\Delta g_T(\tau)$  is the resulting gain change due to the CH and TPA,  $u(s)$  is the unit step function,  $\tau_{ch}$  is the CH relaxation time,  $h_1$  is the contribution of stimulated emission and free-carrier absorption to the CH gain reduction and  $h_2$  is the contribution of TPA.

The dynamically varying slope and curvature of the gain plays a shaping role for pulses in the sub-picosecond range. The first and second order differential net (saturated) gain terms are (Hong *et al.*, 1996),

$$\left. \frac{\partial g(\tau, \omega)}{\partial \omega} \right|_{\omega_0} = A_1 + B_1 [g_0 - g(\tau, \omega_0)] \quad (7)$$

$$\left. \frac{\partial^2 g(\tau, \omega)}{\partial \omega^2} \right|_{\omega_0} = A_2 + B_2 [g_0 - g(\tau, \omega_0)] \quad (8)$$

$$g(\tau, \omega_0) = g_N(\tau, \omega_0) / f(\tau) + \Delta g_T(\tau, \omega_0) \quad (9)$$

where,  $A_1$  and  $A_2$  are the slope and curvature of the linear gain at  $\omega_0$ , respectively, while  $B_1$  and  $B_2$  are constants describing changes in  $A_1$  and  $A_2$  with saturation, as given in (7) and (8).

The gain spectrum of an SOA is approximated by the following second-order Taylor expansion in  $\Delta\omega$ :

$$g(\tau, \omega) = g(\tau, \omega_0) + \Delta\omega \left. \frac{\partial g(\tau, \omega)}{\partial \omega} \right|_{\omega_0} + \frac{(\Delta\omega)^2}{2} \left. \frac{\partial^2 g(\tau, \omega)}{\partial \omega^2} \right|_{\omega_0} \quad (10)$$

The coefficients  $\left. \frac{\partial g(\tau, \omega)}{\partial \omega} \right|_{\omega_0}$  and  $\left. \frac{\partial^2 g(\tau, \omega)}{\partial \omega^2} \right|_{\omega_0}$  are related to  $A_1, B_1, A_2$  and  $B_2$  by (7) and (8).

Here we assumed the same values of  $A_1, B_1, A_2$  and  $B_2$  as in (Hong *et al.*, 1996) for an AlGaAs/GaAs bulk SOA.

The time derivative terms in (3) have been replaced by the central-difference approximation in order to simulate this equation by the FD-BPM (Das *et al.*, 2000). In simulation, the parameter of bulk SOAs (AlGaAs/GaAs, double heterostructure) with a wavelength of 0.86  $\mu\text{m}$  (Hong *et al.*, 1996) is used and the SOA length is 350  $\mu\text{m}$ . The input pulse shape is sech<sup>2</sup> and is Fourier transform-limited. The detail parameters are listed in Table 1 (Section 3).

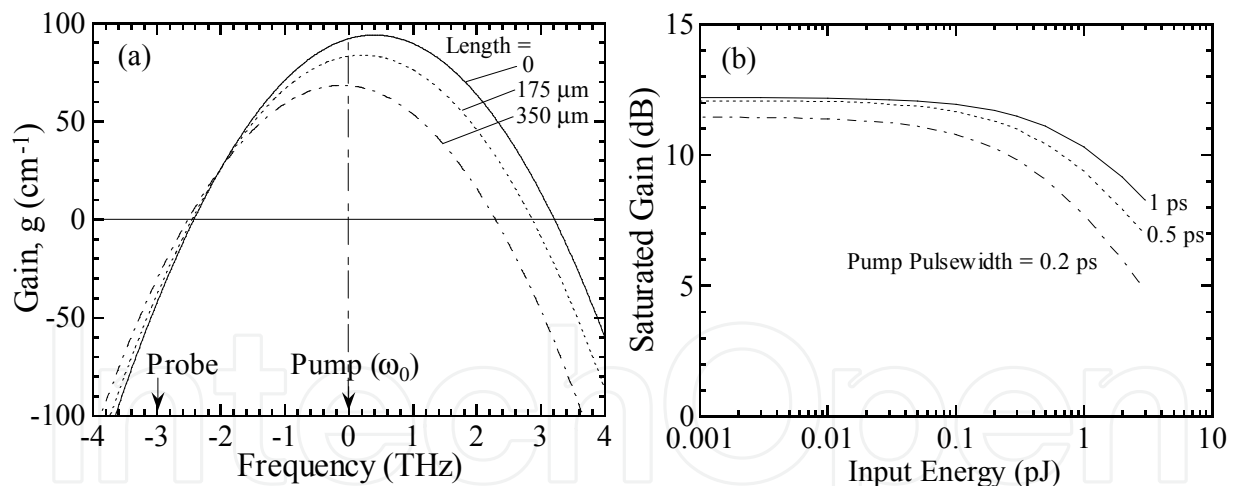


**Figure 2.** (a) The gain spectra given by the second-order Taylor expansion about the center frequency of the pump pulse  $\omega_0$ . The solid line shows the unsaturated gain spectrum (length: 0  $\mu\text{m}$ ), the dotted and the dashed-dotted lines are a saturated gain spectrum at 175  $\mu\text{m}$  and 350  $\mu\text{m}$ , respectively. Here, the input pump pulse pulsewidth is 1 ps and pulse energy is 1 pJ. (b) Saturated gain versus the input pump pulse energy characteristics of the SOA. The saturation energy decreases with decreasing the input pump pulsewidth. The SOA length is 350  $\mu\text{m}$ . The input pulsewidths are 0.2 ps, 0.5 ps, and 1 ps respectively, and a pulse energy of 1 pJ.

The gain spectra of SOAs are very important for obtaining the propagation and wave mixing (FWM and optical phase-conjugation between the input pump and probe pulses)

characteristics of short optical pulses. Figure 2(a) shows the gain spectra given by a second-order Taylor expansion about the pump pulse center frequency  $\omega_0$  with derivatives of  $g(\tau, \omega)$  by (7) and (8) (Das *et al.*, 2000). In Fig. 2(a), the solid line represents an unsaturated gain spectrum (length: 0  $\mu\text{m}$ ), the dotted line represents a saturated gain spectrum at the center position of the SOA (length: 175  $\mu\text{m}$ ), and the dashed-dotted line represents a saturated gain spectrum at the output end of the SOA (length: 350  $\mu\text{m}$ ), when the pump pulsewidth is 1 ps and input energy is 1 pJ. These gain spectra were calculated using (1), because, the waveforms of optical pulses depend on the propagation distance (i.e., the SOA length). The spectra of these pulses were obtained by Fourier transformation. The “local” gains at the center frequency at  $z = 0, 175,$  and  $350 \mu\text{m}$  were obtained from the changes in the pulse intensities at the center frequency at around those positions (Das *et al.*, 2001). The gain at the center frequency in the gain spectrum was approximated by the second-order Taylor expression series. As the pulse propagates in the SOA, the pulse intensity increases due to the gain of the SOA. The increase in pulse intensity reduces the gain, and the center frequency of the gain shifts to lower frequencies. The pump frequency is set to near the gain peak, and linear gain  $g_0$  is  $92 \text{ cm}^{-1}$  at  $\omega_0$ . The probe frequency is set  $-3 \text{ THz}$  from for the calculations of FWM characteristics as described below, and the linear gain  $g_0$  is  $-42 \text{ cm}^{-1}$  at this frequency. Although the probe frequency lies outside the gain bandwidth, we selected a detuning of  $3 \text{ THz}$  in this simulation because the FWM signal must be spectrally separated from the output of the SOA. As will be shown later, even for this large degree of detuning, the FWM signal pulse and the pump pulse spectrally overlap when the pulsewidths become short ( $<0.5 \text{ ps}$ ) (Das *et al.*, 2001). The gain bandwidth is about the same as the measured value for an AlGaAs/GaAs bulk SOA (Seki *et al.*, 1981). If an InGaAsP/InP bulk SOA is used we can expect much wider gain bandwidth (Leuthold *et al.*, 2000). With a decrease in the carrier density, the gain decreases and the peak position is shifted to a lower frequency because of the band-filling effect. Figure 2(b) shows the saturated gain versus input pump pulse energy characteristics of the SOA. When the input pump pulsewidth decreases then the small signal gain decreases due to the spectral limit of the gain bandwidth. For the case, when the input pump pulsewidth is short (very narrow, such as 200 fs or lower), the gain saturates at small input pulse energy (Das *et al.*, 2000). This is due to the CH and SHB with the fast response.

Initially, the MNLSE was used by (Hong *et al.*, 1996) for the analysis of “solitary pulse” propagation in an SOA. We used the same MNLSE for the simulation of FWM and optical phase-conjugation characteristics in SOA using the FD-BPM. Here, we have introduced a complex envelope function  $V(\tau, 0)$  at the input side of the SOA for taking into account the two (pump and probe) or more (multi-pump or prove) pulses.

### 2.3. Finite-Difference Beam Propagation Method (FD-BPM)

To solve a boundary value problem using the finite-differences method, every derivative term appearing in the equation, as well as in the boundary conditions, is replaced by the central differences approximation. Central differences are usually preferred because they

lead to an excellent accuracy (Conte & Boor, 1980). In the modeling, we used the finite-differences (central differences) to solve the MNLSE for this analysis.

Usually, the fast Fourier transformation beam propagation method (FFT-BPM) (Okamoto, 1992; Brigham, 1988) is used for the analysis of the optical pulse propagation in optical fibers by the successive iterations of the Fourier transformation and the inverse Fourier transformation. In the FFT-BPM, the linear propagation term (GVD term) and phase compensation terms (other than GVD, 1st and 2nd order gain spectrum terms) are separated in the nonlinear Schrödinger equation for the individual consideration of the time and frequency domain for the optical pulse propagation. However, in our model, equation (3) includes the dynamic gain change terms, i.e., the 1st and 2nd order gain spectrum terms which are the last two terms of the right-side in equation (3). Therefore, it is not possible to separate equation (3) into the linear propagation term and phase compensation term and it is quite difficult to calculate equation (3) using the FFT-BPM. For this reason, we used the FD-BPM (Chung & Dagli, 1990; Conte & Boor, 1980; Das *et al.*, 2000; Razagi *et al.*, 2009). If we replace the time derivative terms of equation (3) by the below central-difference approximation, equation (11), and integrate equation (3) with the small propagation step  $\Delta z$ , we obtain the tridiagonal simultaneous matrix equation (12)

$$\frac{\partial}{\partial \tau} V_k = \frac{V_{k+1} - V_{k-1}}{2\Delta\tau}, \quad \frac{\partial^2}{\partial \tau^2} V_k = \frac{V_{k+1} - 2V_k + V_{k-1}}{\Delta\tau^2} \tag{11}$$

where,  $V_k = V(\tau_k)$ ,  $V_{k+1} = V(\tau_k + \Delta\tau)$ , and  $V_{k-1} = V(\tau_k - \Delta\tau)$

$$\begin{aligned} -a_k(z + \Delta z) V_{k-1}(z + \Delta z) + \{1 - b_k(z + \Delta z)\} V_k(z + \Delta z) - c_k(z + \Delta z) V_{k+1}(z + \Delta z) \\ = a_k(z) V_{k-1}(z) + \{1 + b_k(z)\} V_k(z) + c_k(z) V_{k+1}(z) \end{aligned} \tag{12}$$

where,  $k = 1, 2, 3, \dots, n$  and

$$a_k(z) = \frac{\Delta z}{2} \left[ \frac{i\beta_2}{2\Delta\tau^2} + i \frac{1}{4\Delta\tau} \frac{\partial g(\tau, \omega, z)}{\partial \omega} \Big|_{\omega_0, \tau_k} - \frac{1}{4\Delta\tau^2} \frac{\partial^2 g(\tau, \omega, z)}{\partial \omega^2} \Big|_{\omega_0, \tau_k} \right] \tag{13}$$

$$\begin{aligned} b_k(z) = -\frac{\Delta z}{2} \left[ \frac{i\beta_2}{\Delta\tau^2} + \frac{\gamma}{2} + \left( \frac{\gamma_{2p}}{2} + ib_2 \right) |V_k(z)|^2 - \frac{1}{2} g_N(\tau_k, \omega_0, z)(1 + i\alpha_N) \right. \\ \left. - \frac{1}{2} \Delta g_T(\tau_k, \omega_0, z)(1 + i\alpha_T) - \frac{1}{2\Delta\tau^2} \frac{\partial^2 g(\tau, \omega, z)}{\partial \omega^2} \Big|_{\omega_0, \tau_k} \right] \end{aligned} \tag{14}$$

$$c_k(z) = \frac{\Delta z}{2} \left[ \frac{i\beta_2}{2\Delta\tau^2} - i \frac{1}{4\Delta\tau} \frac{\partial g(\tau, \omega, z)}{\partial \omega} \Big|_{\omega_0, \tau_k} - \frac{1}{4\Delta\tau^2} \frac{\partial^2 g(\tau, \omega, z)}{\partial \omega^2} \Big|_{\omega_0, \tau_k} \right] \tag{15}$$

where,  $\Delta\tau$  is the sampling time and  $n$  is the number of sampling. If we know  $V_k(z)$ , ( $k = 1, 2, 3, \dots, n$ ) at the position  $z$ , we can calculate  $V_k(z + \Delta z)$  at the position of  $z + \Delta z$

which is the propagation of a step  $\Delta z$  from position  $z$ , by using equation (12). It is not possible to directly calculate equation (12) because it is necessary to calculate the left-side terms  $a_k(z + \Delta z)$ ,  $b_k(z + \Delta z)$ , and  $c_k(z + \Delta z)$  of equation (12) from the unknown  $V_k(z + \Delta z)$ . Therefore, we initially defined  $a_k(z + \Delta z) \equiv a_k(z)$ ,  $b_k(z + \Delta z) \equiv b_k(z)$ , and  $c_k(z + \Delta z) \equiv c_k(z)$  and obtained  $V_k^{(0)}(z + \Delta z)$ , as the zero-th order approximation of  $V_k(z + \Delta z)$  by using equation (12). We then substituted  $V_k^{(0)}(z + \Delta z)$  in equation (12) and obtained  $V_k^{(1)}(z + \Delta z)$  as the first order approximation of  $V_k(z + \Delta z)$  and finally obtained the accurate simulation results by the iteration as used in (Brigham, 1988; Chung & Dagli, 1990; Das *et al.*, 2000; Razagi *et al.*, 2009).

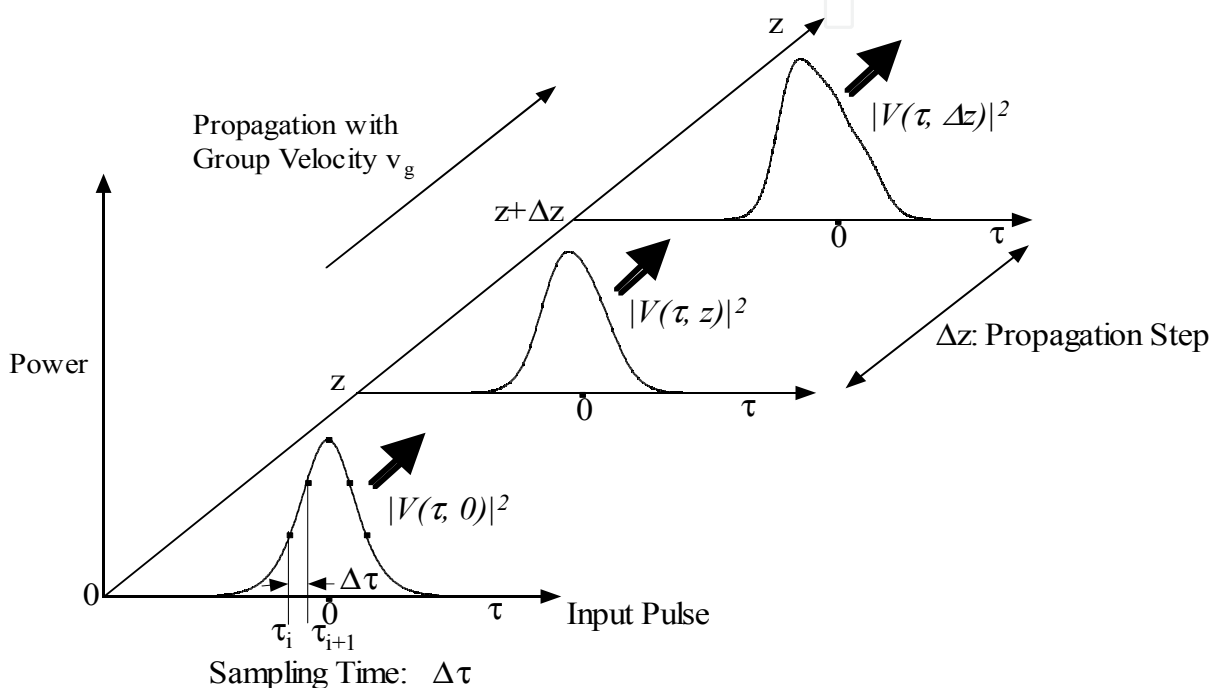


**Figure 3.** A simple schematic diagram of FD-BPM in the time domain, where,  $\tau (= t - z/v_g)$  is the local time, which propagates with the group velocity  $v_g$  at the center frequency of an optical pulse and  $\Delta\tau$  is the sampling time, and  $z$  is the propagation direction and  $\Delta z$  is the propagation step.

Figure 3 shows a simple schematic diagram of the FD-BPM in time domain. Here,  $\tau (= t - z/v_g)$  is the local time, which propagates with the group velocity  $v_g$  at the center frequency of an optical pulse and  $\Delta\tau$  is the sampling time.  $z$  is the propagation direction and  $\Delta z$  is the propagation step. With this procedure, we used up to 3-rd time iteration for more accuracy of the simulations.

The FD-BPM (Conte & Boor, 1980; Chung & Dagli, 1990; Das *et al.*, 2000; Razagi *et al.*, 2009a & 2009b) is used for the simulation of several important characteristics, namely, (1) single pulse propagation in SOAs (Das *et al.*, 2008; Razaghi *et al.*, 2009a & 2009b), (2) two input pulses propagating in SOAs (Das *et al.*, 2000; Connelly *et al.*, 2008), (3) Optical DEMUX characteristics of multi-probe or pump input pulses based on FWM in SOAs (Das *et al.*, 2001), (4) Optical phase-conjugation characteristics of picosecond FWM signal in SOAs (Das

*et al.*, 2001), and (5) FWM conversion efficiency with optimum time-delays between the input pump and probe pulses (Das *et al.*, 2007).

## 2.4. Nonlinear pulse propagation model in SOAs

Nonlinear optical pulse propagation in SOAs has drawn considerable attention due to its potential applications in optical communication systems, such as a wavelength converter based on FWM and switching. The advantages of using SOAs include the amplification of small (weak) optical pulses and the realization of high efficient FWM characteristics.

For the analysis of optical pulse propagation in SOAs using the FD-BPM in conjunction with the MNLSE, where several parameters are taken into account, namely, the group velocity dispersion, SPM, and TPA, as well as the dependencies on the CD, CH, SHB and their dispersions, including the recovery times in an SOA (Hong *et al.*, 1996). We also considered the gain spectrum (as shown in Fig. 2). The gain in an SOA was dynamically changed depending on values used for the carrier density and carrier temperature in the propagation equation (i.e., MNLSE).

Initially, (Hong *et al.*, 1996) used the MNLSE for the simulation of optical pulse propagation in an SOA by FFT-BPM (Okamoto, 1992; Brigham, 1988) but the dynamic gain terms were changing with time. The FD-BPM is capable to simulate the optical pulse propagation taking into consideration the dynamic gain terms in SOAs (Das *et al.*, 2000 & 2007; Razaghi *et al.*, 2009a & 2009b; Aghajanpour *et al.*, 2009). We used the modified MNLSE for nonlinear optical pulse propagation in SOAs by the FD-BPM (Chung & Dagli, 1990; Conte & Boor, 1980). We used the FD-BPM for the simulation of optical phase-conjugation characteristics of picosecond FWM signal pulses in SOAs.

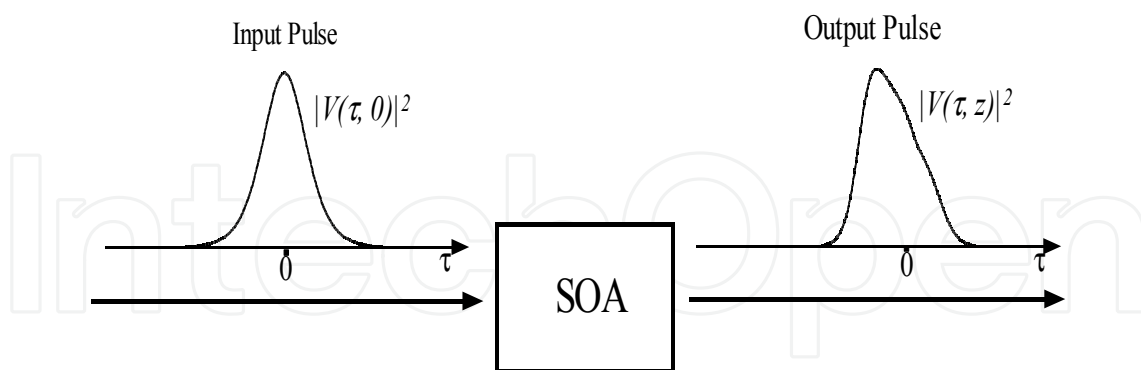


**Figure 4.** A simple schematic diagram for the simulation of nonlinear single pulse propagation in SOA. Here,  $|V(\tau, 0)|^2$  is the input ( $z = 0$ ) pulse intensity and  $|V(\tau, z)|^2$  is the output pulse intensity (after propagating a distance  $z$ ) of SOA.

Figure 4 illustrates a simple model for the simulation of nonlinear optical pulse propagation in an SOA. An optical pulse is injected into the input side of the SOA ( $z = 0$ ). Here,  $\tau$  is the local time,  $|V(\tau, 0)|^2$  is the intensity (power) of input pulse ( $z = 0$ ) and  $|V(\tau, z)|^2$  is the intensity (power) of the output pulse after propagating a distance  $z$  at the output side of

SOA. We used this model to simulate the FWM and optical phase-conjugation characteristics in SOAs.

### 3. FWM characteristics between optical pulses in SOAs

In this section, we will discuss the FWM characteristics between optical pulses in SOAs. When two optical pulses with different central frequencies  $f_p$  (pump) and  $f_q$  (probe) are injected simultaneously into the SOA, an FWM signal is generated at the output of the SOA at a frequency of  $2f_p - f_q$  (as shown in Fig. 5). For the analysis (simulation) of FWM characteristics, the total input pump and probe pulse,  $V_{in}(\tau)$ , is given by the following equation

$$V_{in}(\tau) = V_p(\tau) + V_q(\tau)\exp(-i2\pi\Delta f\tau) \quad (16)$$

where,  $V_p(\tau)$  and  $V_q(\tau)$  are the complex envelope functions of the input pump and probe pulses respectively,  $\tau (= t - z/v_g)$  is the local time that propagates with group velocity  $v_g$  at the center frequency of an optical pulse,  $\Delta f$  is the detuning frequency between the input pump and probe pulses and expressed as  $\Delta f = f_p - f_q$ . Using the complex envelope function of (16), we solved the MNLSE and obtained the combined spectrum of the amplified pump, probe and the generated FWM signal at the output of SOA.

For the simulations, we used the parameters of a bulk SOA (AlGaAs/GaAs, double heterostructure) at a wavelength of  $0.86 \mu\text{m}$ . The parameters are listed in Table 1 (Hong *et al.*, 1996; Das *et al.*, 2000). The length of the SOA was assumed to be  $350 \mu\text{m}$ . All the results were obtained for a propagation step  $\Delta z$  of  $5 \mu\text{m}$ . We confirmed that for any step size less than  $5 \mu\text{m}$  the simulation results were almost identical (i.e., independent of the step size).

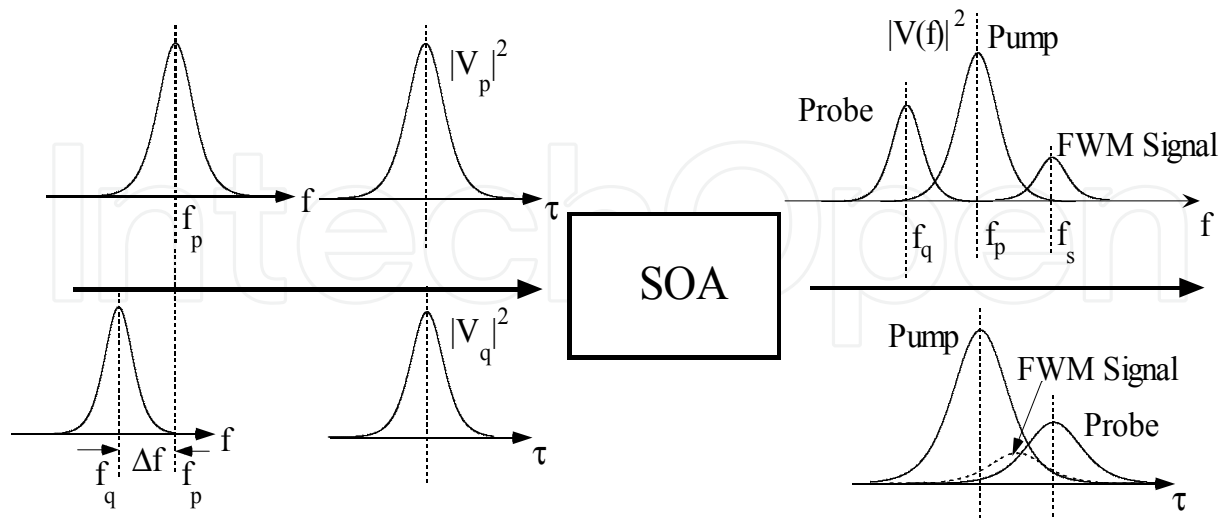


**Figure 5.** A simple schematic diagram for the simulation of FWM characteristics between pump and probe pulses in SOAs. The input pump and probe pulses with the center frequency of  $f_p$  and  $f_q$  are injected into the SOA. The pump and probe pulse detuning is  $\Delta f$ . The FWM signal is generated at the output of the SOA.

Name of the Parameters	Symbols	Values	Units
Length of SOA	L	350	$\mu\text{m}$
Effective area	A	5	$\mu\text{m}^2$
Center frequency of the pulse	$f_0$	349	THz
Linear gain	$g^0$	92	$\text{cm}^{-1}$
Group velocity dispersion	$\beta_2$	0.05	$\text{ps}^2 \text{cm}^{-1}$
Saturation energy	$W_s$	80	pJ
Linewidth enhancement factor due to the CD	$\alpha_N$	3.1	
Linewidth enhancement factor due to the CH	$\alpha_T$	2.0	
The contribution of stimulated emission and FCA to the CH gain reduction	$h_1$	0.13	$\text{cm}^{-1} \text{pJ}^{-1}$
The contribution of TPA	$h_2$	126	$\text{fs cm}^{-1} \text{pJ}^{-2}$
Carrier lifetime	$\tau_s$	200	ps
CH relaxation time	$\tau_{\text{ch}}$	700	fs
SHB relaxation time	$\tau_{\text{shb}}$	60	fs
SHB saturation power	$P_{\text{shb}}$	28.3	W
Linear loss	$\gamma$	11.5	$\text{cm}^{-1}$
Instantaneous nonlinear Kerr effect	$n_2$	-0.70	$\text{cm}^2 \text{TW}^{-1}$
TPA coefficient	$\gamma_{2P}$	1.1	$\text{cm}^{-1} \text{W}^{-1}$
Parameters describing second-order Taylor expansion of the dynamically gain spectrum	$A_1$ $B_1$ $A_2$ $B_2$	0.15 -80 -60 0	$\text{fs } \mu\text{m}^{-1}$ fs $\text{fs}^2 \mu\text{m}^{-1}$ $\text{fs}^2$

**Table 1.** Simulation parameters of a bulk SOA (AlGaAs/GaAs, double heterostructure) (Hong *et al.*, 1996; Das *et al.*, 2000).

For the simulation of optical phase-conjugate characteristics in SOAs, we used the above model (Fig. 5). Fig. 5 shows a simple schematic diagram illustrating the simulation of the FWM characteristics in an SOA between short optical pulses. In SOA, the FWM signal is generated by mixing between the input pump and probe pulses, whose frequency appears at the symmetry position of the probe pulse with respect to the pump. For our simulation (as shown in Fig. 7), we have selected the detuning frequency between the input pump and probe pulses to +3 THz. The generated FWM signal is filtered using an optical narrow bandpass filter from the optical output spectrum containing the pump and probe signal. Here, the pass-band of the filter is set to be from +2 THz to +4 THz, i.e., a bandwidth of 2 THz is used. The shape of the pass-band was assumed to be rectangular.

## 4. Optical phase-conjugation of picosecond FWM signals in SOAs

### 4.1. Chirp of FWM signal pulses for Fourier transform-limited input pulses

In this sub-section, first, we obtain the frequency shift characteristics of FWM signal pulses for Fourier transform-limited input pulses. Fig. 6(a) shows the normalized output power of the pump, probe and FWM signal pulses. Fig. 6(b) shows the center frequency shifts of these pulses. Here, the input pump and probe pulses are Fourier transform limited (non-chirped) Gaussian pulses with a pulsewidth of 2 ps (full width at half maximum: FWHM). The pump-probe detuning is +3 THz. The input pump and probe pulse energy levels are 1 pJ and 0.1 pJ, respectively. The solid, dotted, and dotted-broken curves represent the pulse waveforms of the pump, probe, and generated FWM signal pulses, respectively. We have obtained these output waveforms by the method that have reported by Das et al., (Das et al., 2000). The output waveforms of the pump and probe pulses are close to the input waveforms. However, the peak position of the pump pulse is slightly shifted toward the leading edge due to the gain saturation of the SOA (Shtaif & Eisenstein, 1995; Das et al., 2000). This is because the pulses have a larger gain at the leading edge than at the trailing edge. The pulsewidth of the FWM signal becomes narrower than that of the pump and probe pulses, because the FWM signal intensity is proportional to  $I_p^2 I_q$ , where  $I_p$  is the pump pulse intensity and  $I_q$  is the probe pulse intensity (Das et al., 2000).

The frequency shift characteristics of the pump, probe, and FWM signal pulses are shown in Fig. 6(b). The frequency shift of the FWM signal pulse is plotted for output power, which is greater than 1% of the output peak power. The vertical axis indicates the frequency shifts of the output pulses from the center frequencies of each input pulse. Two components of frequency shifts can be observed; negative frequency shift in the vicinity of the pulse peaks, and a frequency shift that is almost constant with time. In the vicinity of the pulse peaks, all the mixing pulses have negative pulse chirp, indicating that the pulse spectra are mainly red-shifted. A similar frequency shift was reported by Tang & Shore (Tang & Shore, 1999) for SOAs operating at a wavelength of 1.55  $\mu\text{m}$  and attributed to the self- and cross- phase modulation under gain saturation. The origin of another frequency shift that is almost constant with time may be the effect of the gain spectrum of the SOA. The pump pulse frequency was set to near the gain peak. Therefore, both the higher and lower frequency components of the pump pulse have about the same optical gain. Thus the frequency of the pulse does not shift during the propagation in the SOA except for the frequency shift caused by the self- and cross- phase modulation as mentioned above. However, the probe pulse frequency was set at -3 THz from the center frequency of the pump pulse. Therefore, the higher frequency component of the probe pulse was enhanced more than the lower frequency component due to the gain spectrum, and the frequency of the output probe pulse is shifted toward the higher frequency side. This gain spectrum effect caused a +25 GHz shift in the probe pulses. The FWM signal is obtained at about +3 THz from the center frequency of the pump pulse. The lower frequency component of the FWM signal pulse was enhanced more than the higher frequency component. In addition, the probe pulse was

shifted toward the higher frequency side. Therefore, the center frequency of the FWM signal pulse is shifted by about  $-35$  GHz.

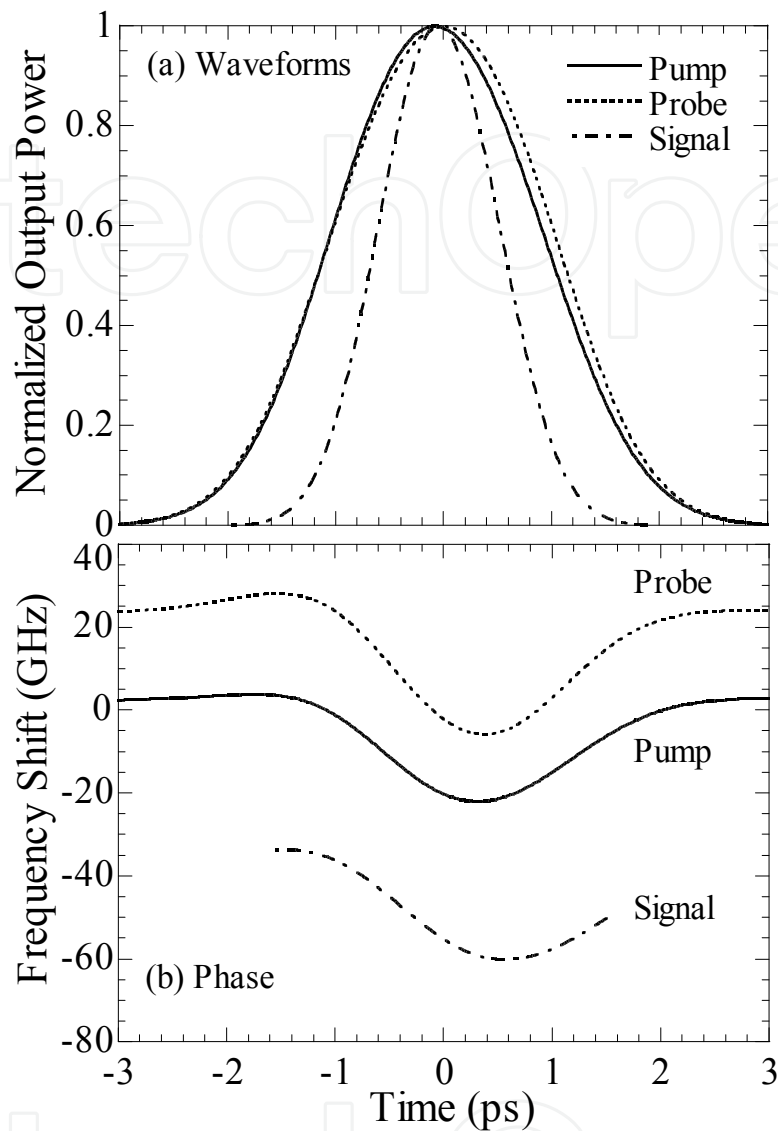


**Figure 6.** Normalized output power (a) and frequency shift (b) of the pump, probe, and generated FWM signal pulses. Input pump and probe pulses are Fourier transform-limited Gaussian shape with a pulsewidth of 2 ps (FWHM), detuning of the input pump and probe pulse is +3 THz. The input pump and probe energy levels are 1 pJ and 0.1 pJ, respectively.

#### 4.2. Optical phase-conjugate characteristics for linearly-chirped input probe pulse

In this sub-section, we have analyzed the optical phase-conjugate characteristics of the FWM signal pulses. The outline of our simulation model, which is similar to the experimental setup used by Kikuchi & Matsumura (Kikuchi & Matsumura, 1998), is the following one, as shown in Fig. 7, the Fourier transform-limited optical pulse is linearly-chirped by transmission through a fiber (Fiber I) and then injected into the SOA as the probe pulse

together with a pump pulse. The FWM signal is generated by the mixing of the probe pulse and the pump pulse, and selected by an optical narrow band-pass filter. The FWM signal is then transmitted through another fiber (Fiber II) that has the same GVD as Fiber I and is an appropriate length.

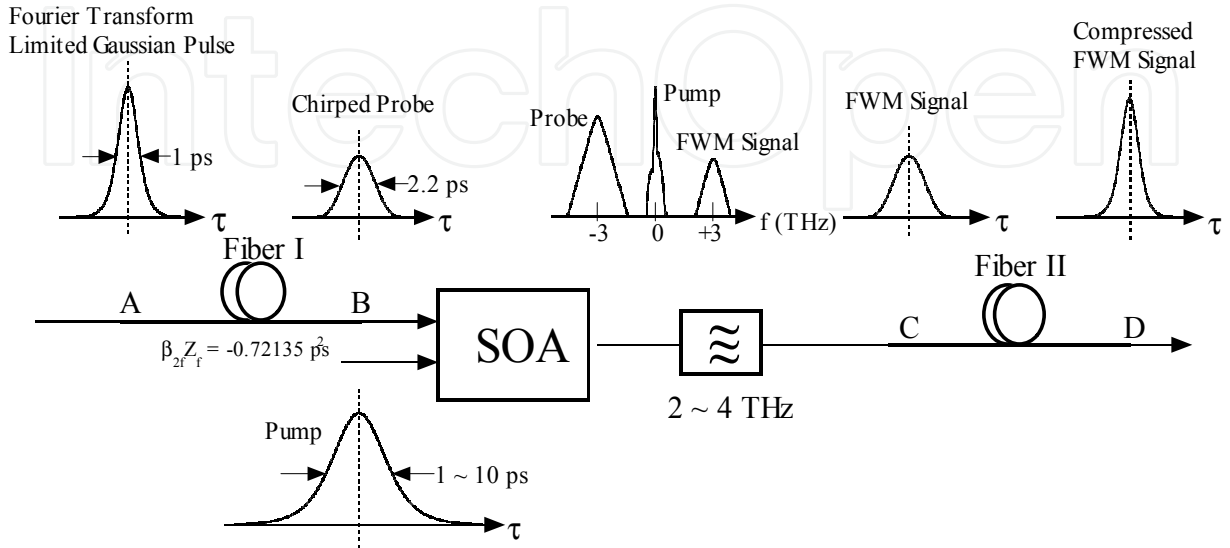


**Figure 7.** A simple schematic diagram for the simulation of optical phase-conjugate characteristics of picosecond FWM signal pulses in SOAs. Fourier transform-limited Gaussian optical pulse is linearly-chirped by transmitting through a fiber (Fiber I) and injected into the SOA as the probe pulse together with a pump pulse. The FWM signal is generated by the mixing of the chirped-probe pulse and the pump pulse, and it is selected by an optical narrow band-pass filter. Then, the FWM signal is transmitted through the fiber (Fiber II) with the same GVD value as Fiber I and the appropriate fiber length.

We have assumed that the input probe pulse is the Fourier transform-limited Gaussian pulse with a pulsewidth of 1 ps (FWHM). Therefore, the incident field is given by Agrawal (Agrawal, 1995; Das *et al.*, 2001)

$$E(0, T) = \exp\left[-\frac{T^2}{2T_0^2}\right] \quad (17)$$

where,  $T_0$  is the half-width at the  $1/e$ -intensity (power) point and 0.60056 ps in this case. The input probe pulse energy is chosen to be 0.1 pJ. This unchirped Gaussian pulse has propagated through the fiber (length  $Z_f$ ) from position A to position B in Fig. 7 and is chirped by the second-order GVD of the fiber, and the duration of the pulse is broadened. The spectrum of the broadened pulse at position B is calculated using the following equation (Agrawal, 1995; Das *et al.*, 2001)

$$\tilde{E}(Z_f, \omega) = \tilde{E}(0, \omega) \exp\left[\frac{i}{2} \beta_{2f} \omega^2 Z_f\right] \quad (18)$$

where,  $\tilde{E}(0, \omega)$  is the Fourier transform of the incident field given by equation (17) at  $Z_f = 0$  (at position A of Fig. 7),  $\omega = 2\pi(f - f_q)$ ,  $f_q$  is the center frequency of the probe pulse, and  $\beta_{2f}$  is the second-order GVD of the fiber. Equation (18) shows that GVD changes the phase of each spectral component of the pulse by an amount that depends on the frequency and the propagation distance. Even though such phase changes do not affect the pulse spectrum, they can modify the pulse shape. Taking the inverse Fourier transform of the Eq. (18), the broadened pulse can be calculated at position B of Fig. 7 using the following equation (Agrawal, 1995; Das *et al.*, 2001):

$$E(Z_f, T) = \frac{1}{2\pi} \int_{-\infty}^{\infty} \tilde{E}(0, \omega) \exp\left[\frac{i}{2} \beta_{2f} \omega^2 Z_f - i\omega T\right] d\omega$$

$$= \frac{T_0}{\left(T_0^2 - i\beta_{2f} Z_f\right)^{1/2}} \exp\left[-\frac{T^2}{\left(T_0^2 - i\beta_{2f} Z_f\right)}\right] \quad (19)$$

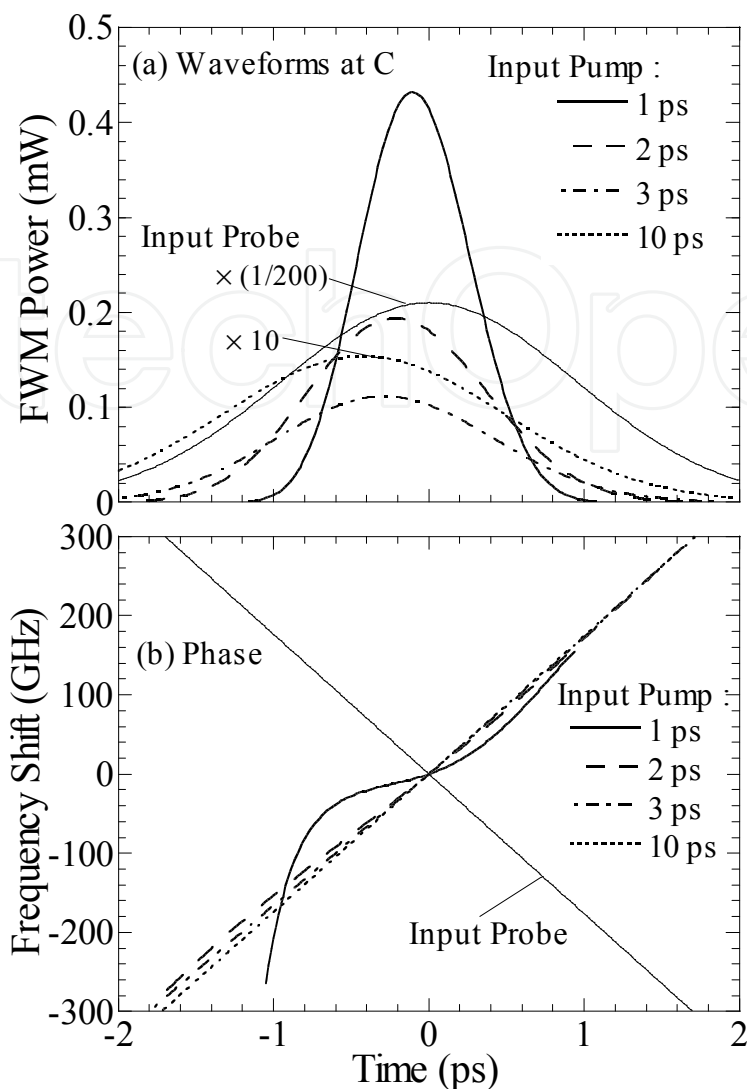
A Gaussian pulse preserves its shape on propagation, yet its width increases and becomes (Agrawal, 1995; Das *et al.*, 2001):

$$T_b = T_0 \left[1 + \left(Z_f/L_D\right)^2\right]^{1/2} \quad (20)$$

where the dispersion length  $L_D = T_0^2 / |\beta_{2f}|$ . The input probe pulse is chirped by the Fiber I with  $\beta_{2f} Z_f = 2\beta_{2f} L_D = -0.72135 \text{ ps}^2$  and is broadened to approximately 2.2 ps.

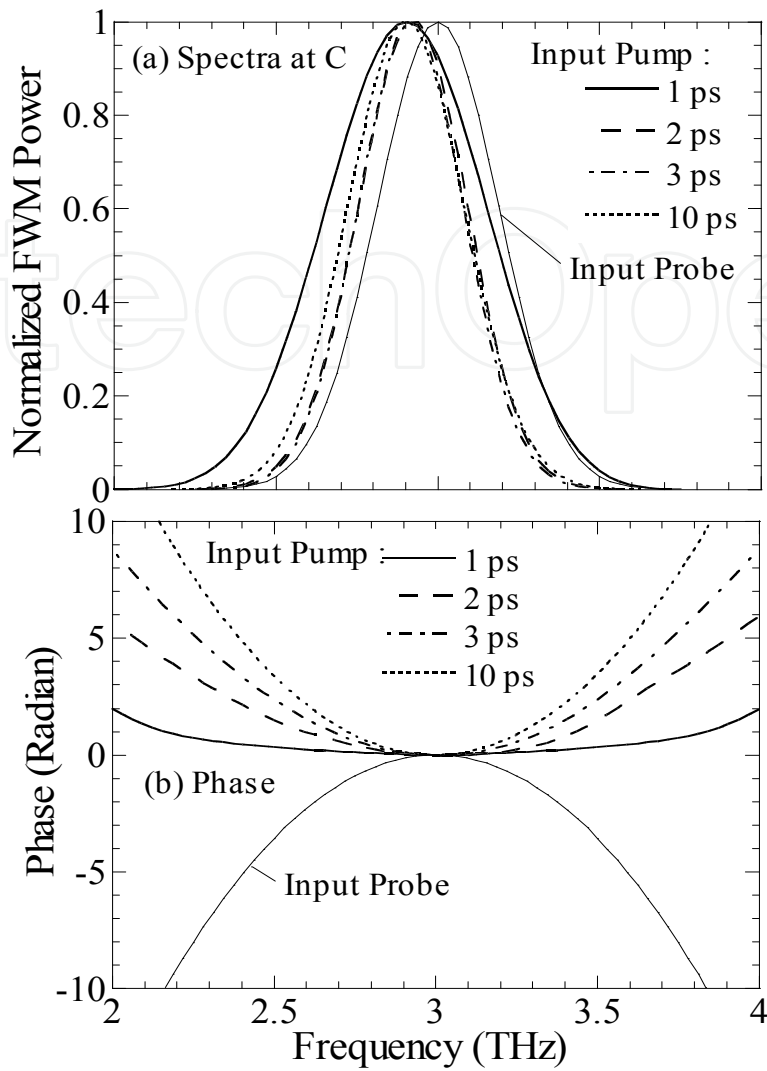
The FWM signal generated by the chirped probe pulse is expressed by Eq. (18) and the Fourier transform-limited Gaussian pump pulses, is obtained from the output facet of a 350  $\mu\text{m}$  length SOA. The detuning between the input pump and the probe pulses is set at 3 THz. The FWM signal is obtained by taking the spectral component between +2 THz and +4 THz (i.e., the bandwidth of the optical filter is 2 THz).

Figure 8 shows the waveforms and the frequency shift of the FWM signal at the output end of the SOA, shown as position C in Fig. 7 together with those of the input probe pulse. The input probe pulse is a chirped Gaussian pulse with a pulsewidth of 2.2 ps (FWHM), as described above, and with an energy of 0.1 pJ. The input pump pulses are the Fourier transform-limited Gaussian pulses with pulsewidths of 1 ps, 2 ps, 3 ps, and 10 ps. The pulsewidth of the FWM signal is increased in step with the increase in the pump pulsewidth. The peak positions of the FWM signals are slightly shifted toward the leading edge due to the gain spectrum of the SOA. As shown in Fig. 8(b) later, the frequency of the probe pulse is linearly chirped from higher frequencies to lower frequencies. As the probe pulse frequency is set to the low frequency side of the SOA gain spectrum, the probe pulse has a larger gain at its leading edge. The center frequency shift of the FWM signal pulses at the output end of the SOA for different input pump pulsewidths is shown in Fig. 8(b), demonstrating the frequency shift of the chirped probe pulse at the input side of the SOA.



**Figure 8.** Waveforms and frequency shift of the generated FWM signal at the output end of the SOA shown as the position C in Fig. 7 together with those of the input probe pulse.

We have defined zero frequency shift to be that at 0 ps. If the SOA acts as an ideal optical phase conjugator, the frequency shift of the FWM signal should be symmetrical with that of the input probe pulse. The frequency shift of the FWM signal is plotted for output power, which is greater than 1% of the FWM peak power. For the input pump pulsewidth of 10 ps, the frequency shift of the FWM signal is very similar to the symmetrical shape of the input probe. With a decrease in the input pump pulsewidth, the symmetry breaks due to a change in the refractive index of the SOA, as caused by the pump pulse. For a 1 ps pump pulsewidth, the symmetry is strongly degraded. In the model, we have taken into account carrier depletion, CH, SHB, and the instantaneous nonlinear Kerr effect, as the origins of nonlinear refractive index changes. For the case of a 1 ps pump pulse, the anomalous frequency shift at the leading edge of the pump pulse primarily originates from the Kerr effect. By contrast, all mechanisms contribute to the frequency shift at the trailing edge. As a result of this simulation, we found that the phase-conjugate characteristics are almost entirely preserved, even for a 2 ps input pump pulsewidth.



**Figure 9.** Spectra and phase in the frequency domain of the FWM signal at the output end of the SOA shown as the position C in Fig. 7 together with those of the probe input pulse.

The spectra and phase of the generated FWM signal in the frequency domain at the output end of the SOA shown as the position C in Fig. 7, together with the spectra and phase of the input probe pulse, as shown in Fig. 9. Although the center frequency of the probe pulse is at  $-3$  THz, the spectrum and the phase of the input probe pulse are plotted at  $+3$  THz to aid for comparison with the FWM signal pulse. We assumed a Fourier transform-limited Gaussian pulse as the input of the fiber, and so the power spectrum does not change during the propagation in the fiber. Therefore, the input probe spectrum is the same as the input pulse to the fiber. The phase of the probe pulse in the frequency domain should vary according to  $(f - f_q)^2$  against the frequency  $f$ . Here,  $f_q$  is the center frequency of the probe pulse. The results shown in Fig. 9 are in complete agreement with the above considerations. The peak frequencies of the FWM spectra are shifted to the lower frequency side of the frequency spectra. These shifts are mainly due to the SPM caused by the gain saturation effect (Das et al., 2000; Das et al., 2001). The phase of the

FWM spectra at the output of the SOA is shown in Fig. 9(b). If the SOA acts as an ideal optical phase conjugator, the phase of the FWM spectra should be symmetrical with that of the input probe pulse spectrum. From the figure, the phase of the FWM signal for a pump pulsewidth of 10 ps is almost symmetrical to the phase of the input probe pulse. With a decrease in the input pump pulsewidth, this symmetry decreases. This tendency is the same as that found for time domain (see Fig. 9(a)).

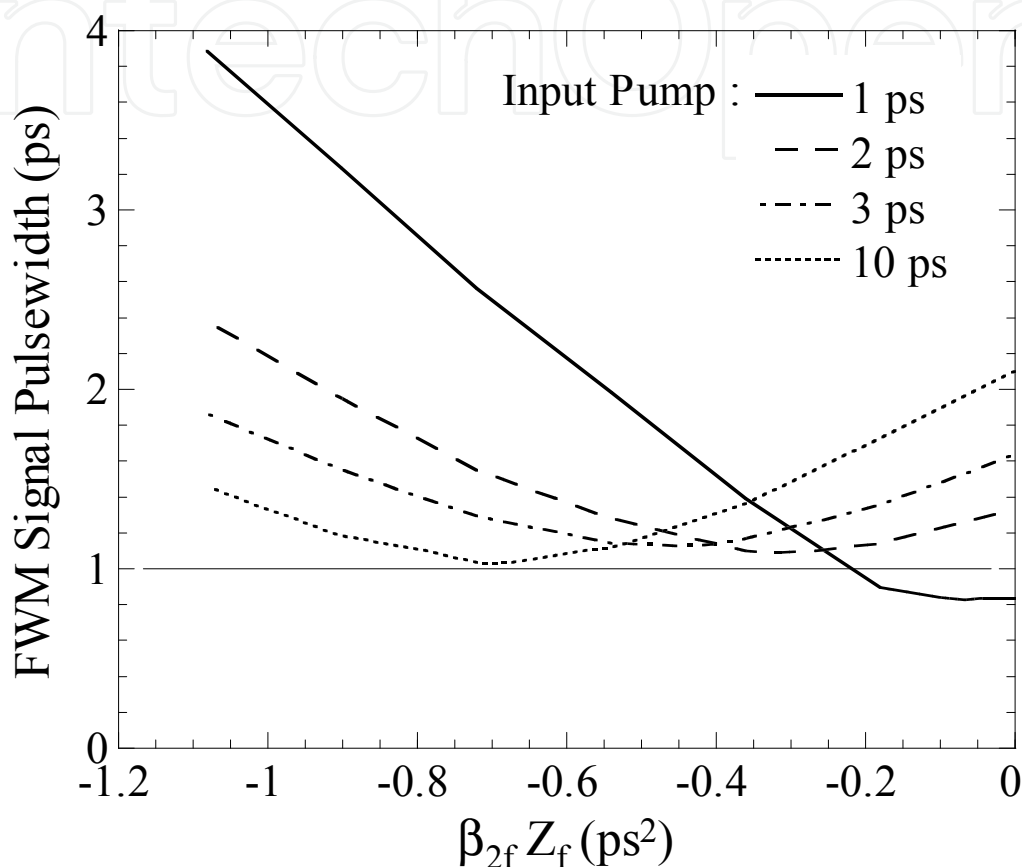


**Figure 10.** FWM signal pulsewidth versus the  $\beta_{2f} Z_f$  value characteristics at position D in Fig. 7.

The chirped pulse can be easily compressed using the phase-conjugate characteristics of the FWM signal pulse and the second-order GVD of a fiber. Figure 10 shows the pulsewidth of the FWM signal versus the  $\beta_{2f} Z_f$  value characteristics at position D in Fig. 7. For a 10 ps pump pulse, the SOA acts as a nearly ideal phase conjugator within the confines of reversing the chirp of optical pulses. The pulsewidth of the output pulse becomes the shortest, 1.03 ps, at  $\beta_{2f} Z_f = -0.70$  ps<sup>2</sup> (Dijaili et al., 1990; Kikuchi & Matsumura, 1998), which is slightly smaller (~3%) than the assumed  $\beta_{2f} Z_f$  of the input fiber we assumed. The shortest pulsewidth compresses to 1 ps, which is equal to the input pulsewidth of the Fourier transform-limited probe pulse. This result confirms that the SOA acts as a nearly ideal phase conjugator (i.e., reverse chirp) when the input pump pulsewidth is relatively long (10 ps). When the input pump pulsewidth becomes shorter, the  $\beta_{2f} Z_f$  value for obtaining the shortest pulsewidth becomes smaller, and the shortest pulsewidth becomes

wider than the input pulsewidth of 1 ps. For example, for a 3 ps pump pulse, the shortest pulsewidth is  $\sim 1.1$  ps which is obtained at  $\beta_{2f}Z_f = -0.45$  ps<sup>2</sup>. This result can be understood as follows: The FWM process acts as both a temporal and a spectral window depending on the pulsewidth and the spectral width of the pulses. By the FWM characteristics described in III-A, the pulsewidth of the FWM signal becomes shorter than the chirped probe pulse. Therefore, only a part of the phase information is copied to the FWM signal. For a 1 ps pump pulse, the temporal window effect is enhanced. In addition, the pump pulse loses phase information due to the optical nonlinear effect that is induced by their strong pulse peak intensity, as shown in Fig. 7. Therefore, the FWM signal pulsewidth becomes less than 1 ps at  $t = 0$  and the shortest FWM signal pulsewidth was obtained for  $\beta_{2f}Z_f = -0.07$  ps<sup>2</sup>.

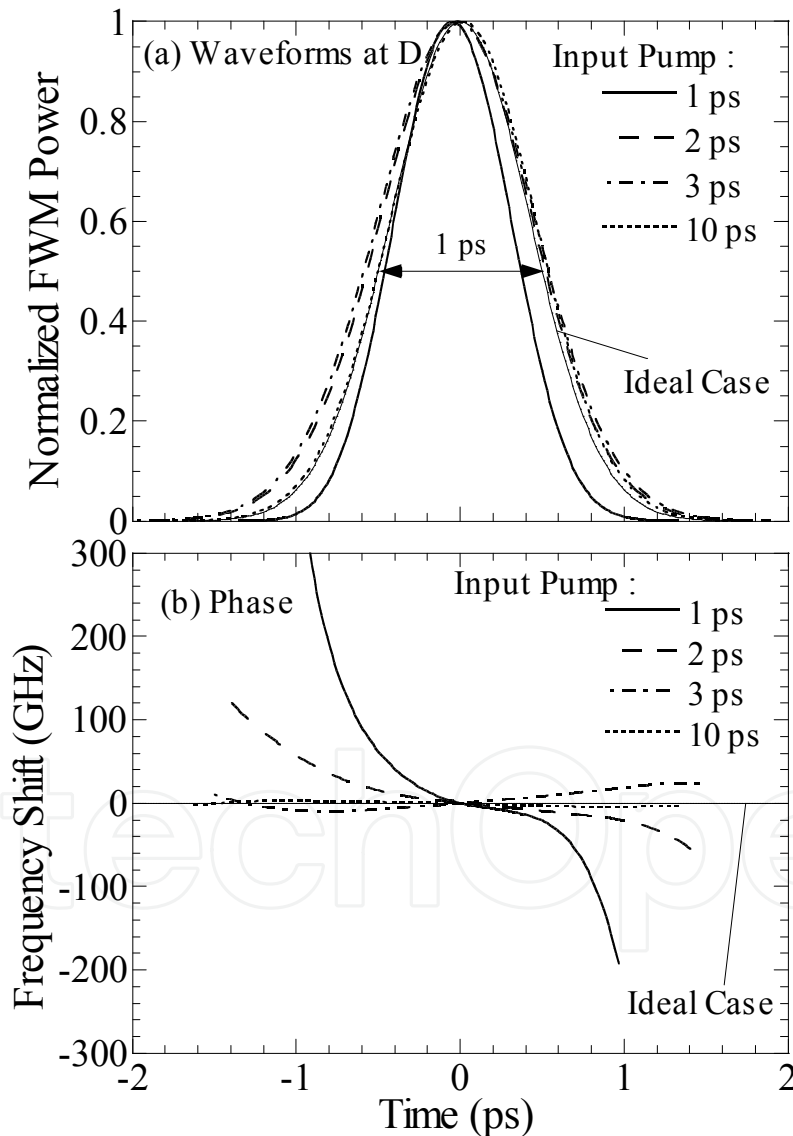


**Figure 11.** Normalized FWM signal waveforms having minimum pulsewidth (a) and the frequency shift (b) at position D in Fig. 7 after the pulse compression by the fiber. This figure also shows those of the input pulse at position A in Fig. 7, which correspond to the case that the SOA acts as the ideal phase conjugation.

Figure 11 shows the normalized FWM signal waveforms with minimum pulsewidth (a), and the frequency shift (b) at the position D in Fig. 7 after the pulse compression by the same fiber. The normalized waveform of the input pulse at position A in Fig. 7 is also shown, corresponds to the case where the SOA acts as an ideal phase conjugator. The normalized waveforms of the FWM signal pulse for various pump pulsewidths are shown in the figure. Although all the FWM signal pulses are compressed to  $\sim 1$  ps when the values of  $\beta_{2f}Z_f$  is optimized, the FWM signal waveform is close to that of the ideal phase conjugator for the longer pump pulse of 10 ps. The frequency shift of the FWM signals after fiber dispersion compensation shows that for the longer pump pulse of 10 ps, the frequency shift becomes nearly zero, which indicates that chirp becomes nearly zero. This suggests that the compressed FWM signal almost becomes a transform-limited pulse. For the pump pulsewidth of 1 ps, the phase of the FWM signal was significantly distorted.

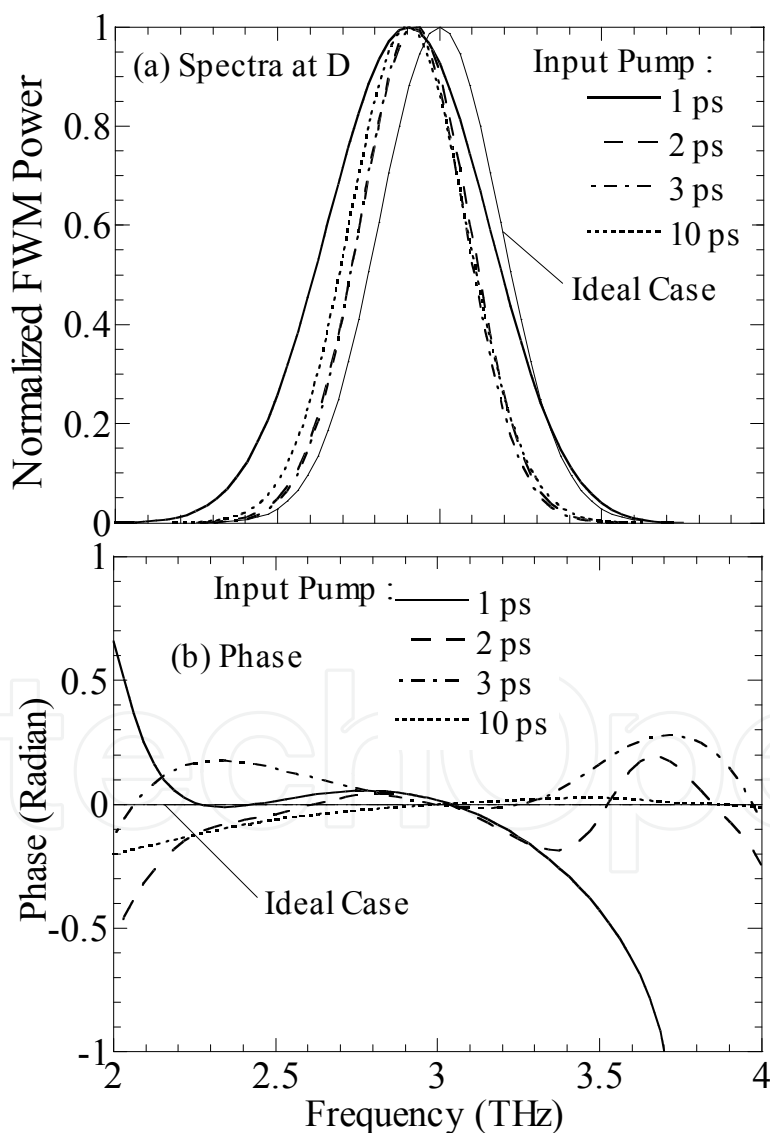


**Figure 12.** Spectra and phase in the frequency domain of the FWM signal pulse at the output end of the dispersion compensation fiber shown as the position D in Fig. 7, together with those for the ideal case.

The spectra and phase in the frequency domain of the FWM signal pulse at the output end of the dispersion compensation fiber, shown as the position D in Fig. 7, are shown in Fig. 12 with the spectra and phase for the ideal case. For the 10 ps pump pulsewidth, the spectrum is almost identical to the ideal case except for the center frequency. The red shift of the center frequency originates from the gain spectrum of the SOAs. For the shorter pump pulse of 1 ps, the spectral width increased because the pulsewidth of the FWM signal becomes short, as shown in Fig. 11(a). From the figure, the output signal phase becomes nearly constant when the input pump pulsewidth is 10 ps. As a result of this simulation (modeling results), we can conclude that pump pulses longer than 10 ps are needed in order to obtain nearly ideal optical phase-conjugate characteristics for the ~2.2 ps chirped pulse.

## 5. Conclusion

We have presented a detail numerical analysis of optical phase-conjugate characteristics of the FWM signal pulses generated in SOAs using the FD-BPM. We have shown that the input pump pulsewidth is an important factor in determining the optical phase-conjugate characteristics of the FWM signal pulse. If we use relatively long input pump pulses, nearly ideal phase-conjugate characteristics, within the confines of reversing the chirp of optical pulses, can be obtained even for very short optical probe pulses. From the simulated example, it has been clarified that the nearly ideal phase-conjugate characteristics are obtained for ~2.2 ps chirped probe pulses using a 10 ps pump pulse. When the pulsewidth of pump pulse decreases, the minimum compressed pulsewidth is obtained using the fiber with a smaller  $\beta_{2f}Z_f$  than that of the input fiber. For much shorter pump pulses such as 1 ps, short FWM signals can be obtained via the gating characteristics of the FWM. However, only a part of the phase information is copied to the FWM signal, and the phase information is lost due to the nonlinear effect. Thus, the pulsewidth is not compressed by propagation through a dispersive medium.

## Author details

Narottam Das

*Department of Electrical and Computer Engineering, Curtin University, Australia  
School of Engineering, Edith Cowan University, Australia*

Hitoshi Kawaguchi

*Graduate School of Materials Science, Nara Institute of Science and Technology, Japan*

Mohammad Razaghi

*Department of Electrical and Computer Engineering, University of Kurdistan, Iran*

## Acknowledgement

The authors would like to thank Dr. T. Kawazoe and Mr. Y. Yamayoshi for their helpful contribution to this work.

## 6. References

- Agrawal, G. P. (1995). *Nonlinear Fiber Optics*. Academic Press, New York. ISBN 0-12-045142-5.
- Agrawal, G. P. & Olsson, N. A. (1989). Self-phase modulation and spectral broadening of optical pulses in semiconductor laser and amplifiers. *IEEE J. Quantum Electron.*, vol. 25, pp. 2297-2306, ISSN 0018-9197.
- Aghajanpour, H.; Ahmadi, V. & Razaghi, M. (2009). Ultra-short optical pulse shaping using semiconductor optical amplifier. *Optics & Laser Technology*, vol. 41, pp. 654-658, ISSN 0030-3992.
- Brigham, E. Oran (1988). *The Fast Fourier Transform and Its Applications*. Englewood Cliffs, N.J.: Prentice-Hall Inc. ISBN 0-13-307505-2.
- Buxens, A.; Poulsen, H. N., Clausen, A. T., & Jeppesen, P. (2000). All-optical OTDM-to-WDM signal-format translation and OTDM add-drop functionality using bidirectional four wave mixing in semiconductor optical amplifier. *Electron. Lett.*, vol. 36, pp. 156-158, ISSN 0013-5194.
- Chung, Y. & Dagli, N. (1990). An Assessment of finite difference beam propagation method. *IEEE J. Quantum Electron.*, vol. 26, pp. 1335-39, ISSN 0018-9197.
- Connelly, M. J.; Barry, L. P., Kennedy, B. F. & Ried, D. A. (2008). Numerical analysis of four-wave mixing between picosecond mode-locked laser pulses in a tensile-strained bulk SOA. *Optical and Quantum Electronics*, vol. 40, pp. 411-418, ISSN 1572-817X.
- Conte, S. D. & Boor, Carl de (1980). *Elementary Numerical Analysis: An Algorithmic Approach*, Third Edition, McGraw-Hill Book Company Co., Singapore. ISBN 0070124477.
- Corchia, A.; Antonini, C., D'Ottavi, A., Mecozzi, A., Martelli, F., Spano, P., Guekos, G., & Dall'Ara, R. (1999). Mid-span spectral inversion without frequency shift for fiber dispersion compensation: A system demonstration. *IEEE Photon. Technol. Lett.*, vol. 11, pp. 275-277, ISSN 1041-1135b. 1999.
- Das, N. K. (2000). *Numerical simulations of four-wave mixing among short optical pulses in semiconductor optical amplifiers by the beam propagation method*. PhD dissertation, Yamagata University, Japan.
- Das, N. K.; Yamayoshi, Y. & Kawaguchi, H. (2000). Analysis of basic four-wave mixing characteristics in a semiconductor optical amplifier by beam propagation method. *IEEE J. Quantum Electron.*, vol. 36, pp. 1184-1192, ISSN 0018-9197.
- Das, N. K. & Karmakar, N. C. (2008). Nonlinear propagation and wave mixing characteristics of pulses in semiconductor optical amplifiers. *Microwave and Optical Technology Letters*, vol. 50, pp. 1223-1227, ISSN 0895-2477.
- Das, N. K.; Kawaguchi, H. & Alameh, K. (2011). *Advances in Optical Amplifiers*, Paul Urquhart (Ed.), "Ch. 6: Impact of Pump-Probe Time Delay on the Four-Wave Mixing Conversion Efficiency in SOAs", InTech, Austria. ISBN 978-953-307-186-2.

- Das, N. K.; Karmakar, N. C., Yamayoshi, Y. & Kawaguchi, H. (2007). Four-wave mixing characteristics in SOAs with optimum time-delays between pump and probe pulses," *Microwave and Optical Technology Letters*, vol. 49, pp. 1182-1185, ISSN 0895-2477.
- Das, N. K.; Yamayoshi, Y., Kawazoe, T. & Kawaguchi, H. (2001). Analysis of optical DEMUX characteristics based on four-wave mixing in semiconductor optical amplifiers. *IEEE /OSA J. Lightwave Technol.*, vol. 19, pp. 237-246, ISSN 0733-8724.
- Das, N. K.; Kawazoe, T., Yamayoshi, Y. & Kawaguchi, H. (2001). Analysis of optical phase-conjugate characteristics of picosecond four-wave mixing signals in semiconductor optical amplifiers. *IEEE J. Quantum Electron.*, vol. 37, pp. 55-62, ISSN 0018-9197.
- Das, N. K.; Karmakar, N. C., Yamayoshi, Y. & Kawaguchi, H. (2005). Four-wave mixing characteristics among short optical pulses in semiconductor optical amplifiers with optimum time-delays, *Proceedings of the 18th Annual Meeting of the IEEE Lasers and Electro-Optics Society 2005 (IEEE-LEOS2005)*, pp. 127-128, ISBN 0-7803-9217-5, Sydney, NSW, Australia, October 2005, IEEE Press (USA).
- Dienes, A.; Heritage, J. P., Jasti, C. & Hong, M. Y. (1996). Femtosecond optical pulse amplification in saturated media. *J. Opt. Soc. Am. B*, vol. 13, pp. 725-734, ISSN 0740-3224.
- Diez, S.; Schmidt, C., Ludwig, R., Weber, H. G., Obermann, K., Kindt, S., Koltchanov, I. & Petermann, K. (1997). Four-wave mixing in semiconductor optical amplifiers for frequency conversion and fast optical switching. *IEEE J. Sel. Top. Quantum Electron.*, vol. 3, pp. 1131-1145, ISSN 1939-1404.
- Diez, S.; Mecozzi, A. & Mørk, J. (1999). Bit rate and pulse width dependence of four-wave mixing of short pulses in semiconductor optical amplifiers. *Opt. Lett.*, vol. 24, pp. 1675-1677, ISSN: 0146-9592.
- Dijaili, S. P.; Dienes, A., & Smith, J. S. (1990). ABCD matrices for dispersive pulse propagation. *IEEE J. Quantum. Electron.*, vol. 26, pp. 1158-1164, ISSN 0018-9197.
- Ducellier, T. & Bibey, M. B. (1996). Study of optical phase conjugation in bulk travelling wave semiconductor optical amplifier. *IEEE Photon. Technol. Lett.*, vol. 8, pp. 530-32, ISSN 1041-1135.
- Eiselt, M. (1995). Optimum pump pulse selection for demultiplexer application of four-wave mixing in semiconductor laser amplifiers. *IEEE Photon. Technol. Lett.*, vol. 7, pp. 1312-1314, ISSN 1041-1135.
- Gingrich, H. S.; Chumney, D. R., Sun, S.-Z., Hersee, S. D., Lester, L. F. & Brueck, S. R. (1997). Broadly tunable external cavity laser diodes with staggered thickness multiple quantum wells. *IEEE Photon. Technol. Lett.*, vol. 9, pp. 155-157, ISSN 1041-1135.
- Hong, M. Y.; Chang, Y. H., Dienes, A., Heritage, J. P., Delfyett, P. J., Dijaili, Sol & Patterson, F. G. (1996). Femtosecond self- and cross-phase modulation in semiconductor laser amplifiers. *IEEE J. Sel. Top Quantum Electron.*, vol. 2, pp. 523-539, ISSN 1939-1404.

- Inoue, J. & Kawaguchi, H. (1998). Highly nondegenerate four-wave mixing among sub-picosecond optical pulses in a semiconductor optical amplifier," *IEEE Photon. Technol. Lett.*, vol. 10, pp. 349–351, ISSN 1041-1135.
- Kawaguchi, H. & Inoue, J. (1996a). Four-wave mixing among sub-picosecond optical pulses in semiconductor optical amplifier. *Proc. of the 20<sup>th</sup> International Quantum Electronics Conference, IQEC '96*, Tul 105, Sydney, Australia, ISSN.
- Kawaguchi, H. & Inoue, J. (1996b). Wavelength Conversion of sub-picosecond optical pulses by four-wave mixing in a semiconductor optical amplifier. Conference on Laser and Electro-Optics Europe, CLEO/ Europe '96, CBF5, Hamburg, Germany, ISSN: 0-7803-3169-9.
- Kawaguchi, H. & Inoue, J. (1998). Four-wave mixing among sub-picosecond optical pulses in a semiconductor optical amplifier and its applications to optical sampling. *Proc. of SPIE, Physics and Simulation of Optoelectronic Devices VI*, vol. 3283, pp. 447-454, Jan. 26-30, ISSN-13: 978-0819427229.
- Kawanishi, S.; Okamoto, K., Ishii, M., Kamatani, T., Takara, H., & Uchiyama, K. (1997). All-optical time-division-multiplexing on four-wave mixing in a travelling-wave semiconductor laser amplifier. *Electron. Lett.*, vol. 33, pp. 976-977, ISSN 0013-5194.
- Kawanishi, S.; Morioka, T., Kamatani, O., Takara, H., Jacob, J.M., & Saruwatari, M. (1994). 100 Gbit/s all-optical demultiplexing using four-wave mixing in a travelling wave laser diode amplifier. *Electron. Lett.*, vol. 30, pp. 981-982, ISSN 0013-5194.
- Kikuchi, K. & Matsumura, K. (1998). Transmission of 2-ps optical pulses at 1550 nm over 40-km standard fiber using midspan optical phase conjugation in semiconductor optical amplifiers. *IEEE Photon. Technol. Lett.*, vol. 10, pp. 1410-1412, ISSN 1041-1135.
- Kirita, H.; Hashimoto, Y., & Yokoyama, H. (1998). All-optical signal processing at over 100 Gbit/s with nonlinear effects in semiconductor lasers. *Tech. Dig. Int'l. Trop. Workshop on Contemporary Technologies (CPT '98)*, Paper Pc-14, Tokyo, Japan.
- Koltchanov, I.; Kindt, S., Petermann, K., Diez, S., Ludwig, R., Schnabel, R., & Weber, H. G. (1996). Gain dispersion and saturation effects in four-wave mixing in semiconductor laser amplifiers. *IEEE J. Quantum Electron.*, vol. 32, pp. 712-720, ISSN 0018-9197.
- Leuthold, J.; Mayer, M., Eckner, J., Guekos, G., Melchior, H. and Zellweger, Ch. (2000). Material gain of bulk 1.55  $\mu\text{m}$  InGaAsP/InP semiconductor optical amplifiers approximated by a polynomial model. *J. Appl. Phys.*, vol. 87, pp. 618-620, ISSN.
- Marcenac, D. D.; Nasset, D., Kelly, A. E., & Gavriovic, D. (1998). 40 Gbit/s transmission over 103 km of NDSF using polarization independent mid-span spectral inversion by four-wave mixing in a semiconductor optical amplifier. *Electron. Lett.*, vol. 34, pp. 100-101, ISSN 0013-5194.
- Mecozzi, A. & Mørk, J. (1997). Saturation effects in nondegenerate four-wave mixing between short optical pulses in semiconductor laser amplifiers. *IEEE J. Sel. Top Quantum Electron.*, vol. 3, pp. 1190-1207, ISSN 1939-1404.

- Mecozzi, A.; D'Ottavi, A., Iannone, E., & Spano, P. (1995). Four-wave mixing in travelling-wave semiconductor amplifiers. *IEEE J. Quantum Electron.*, vol. 31, pp. 689-699, ISSN 0018-9197.
- Mikami, O.; Noguchi, Y., Yasaka, H., Magari, K. & Kondo, S. (1991). Emission spectral width broadening for InGaAsP/InP superluminescent diodes. *IEE Proc. J Optoelectron.*, vol. 138, pp. 133-137, ISSN: 0267-3932.
- Mørk, J. & Mecozzi, A. (1997). Theory of nondegenerate four-wave mixing between pulses in a semiconductor waveguide. *IEEE J. Quantum Electron.*, vol. 33, pp. 545-555, ISSN 0018-9197.
- Morioka, T.; Takara, H., Kawanishi, S., Uchiyama, K., & Saruwatari, M. (1996). Polarisation-independent demultiplexing up to 200 Gb/s using four-wave mixing in a semiconductor laser amplifier. *Electron. Lett.*, vol. 32, pp. 840-841, ISSN 0013-5194.
- Neset, D.; Marcenac, D. D., Mason, P. L., Kelly, A. E., Bouchoule, S., & Lach, E. (1998). Simultaneous wavelength conversion of two 40 Gbit/s channels using four-wave mixing in a semiconductor optical amplifier. *Electron. Lett.*, vol. 34, pp. 107-108, ISSN 0013-5194.
- Okamoto, K. (1992). *Theory of Optical Waveguides*, Corona Publishing Co., Tokyo; Ch. 7 (in Japanese). ISBN 4-339-00602-5.
- Razaghi, M.; Ahmadi, A., Connelly, M. J. & Madanifar, K. A. (2009a). Numerical modelling of sub-picosecond counter propagating pulses in semiconductor optical amplifiers. *Proceedings of the 9th International Conference on Numerical Simulation of Optoelectronic Devices 2009 (NUSOD' 09)*, pp. 59-60, ISBN 978-1-4244-4180-8, GIST, Gwangju, South Korea, September 2009, IEEE Press (USA).
- Razaghi, M.; Ahmadi, A., & Connelly, M. J. (2009b). Comprehensive finite-difference time-dependent beam propagation model of counter propagating picosecond pulses in a semiconductor optical amplifier. *IEEE/OSA J. Lightwave Technol.*, vol. 27, pp. 3162-3174, ISSN 0733-8724.
- Saleh, A. A. A. & Habbab, I. M. I. (1990). Effects of semiconductor-optical-amplifier nonlinearity on the performance of high-speed intensity-modulation lightwave systems. *IEEE Trans. Commun.*, vol. 38, pp. 839-846, ISSN 0090-6778.
- Sauter, E. G. (1996). *Nonlinear Optics*. John Wiley & Sons, Inc. New York. ISBN 0-471-14860-1.
- Seki, K.; Kamiya, T. and Yanai, H. (1981). Effect of waveguiding properties on the axial mode competition in stripe-geometry semiconductor lasers. *IEEE J. Quantum Electron.*, vol. 17, pp. 706-713, ISSN 0018-9197.
- Shtaif, M. & Eisenstein, G. (1995). Analytical solution of wave mixing between short optical pulses in semiconductor optical amplifier. *Appl Phys. Lett.* 66, pp. 1458-1460, ISSN 0003-6951.
- Shtaif, M.; Nagar, R. & Eisenstein, G. (1995). Four-wave mixing among short optical pulses in semiconductor optical amplifiers. *IEEE Photon Technol. Lett.* 7, pp. 1001-1003. ISSN 1041-1135.

- Shtaif, M. & Eisenstein, G. (1996). Calculation of bit error rates in all-optical signal processing applications exploiting nondegenerate four-wave mixing in semiconductor optical amplifiers. *IEEE/OSA J. Lightwave. Technol.*, vol. 14, pp. 2069-2077, ISSN 0733-8724.
- Summerfield, M. A. & Tucker, S. R. (1995). Noise figure and conversion efficiency of four-wave mixing in semiconductor optical amplifiers. *Electron. Lett.*, vol. 31, pp. 1159-1160, ISSN 0013-5194.
- Set, S. Y.; Yamashita, S., Ibsen, M., Laming, R. I., Nettet, D., Kelly A. E. & Gilbertas, C. (1998). Ultra-high bit rate of optical phase conjugation/ wavelength conversion in NDSF and SOA with novel configuration incorporating inline fibre DFB lasers. *Electron. Lett.*, vol. 34, pp. 1681-83, ISSN 0013-5194.
- Tang, J. M. & Shore, K. A. (1998). Influence of probe depletion and cross-gain modulation on four-wave mixing of picosecond optical pulses in semiconductor optical amplifiers," *IEEE Photon. Technol. Lett.*, vol. 10, pp. 1563-1565, ISSN 1041-1135.
- Tang, J. M. & Shore, K. A. (1999). Active picosecond optical phase compression in semiconductor optical amplifiers. *IEEE J. Quantum. Electron.*, vol. 35, pp. 93-100, ISSN 0018-9197.
- Tang, J. M. & Shore, K. A. (1999). Characteristics of optical phase conjugation of picosecond pulses in semiconductor optical amplifiers. *IEEE J. Quantum. Electron.*, vol. 35, pp. 1032-1040, ISSN 0018-9197.
- Tang, J. M.; Spencer, P. S. & Shore, K. A. (1998). The influence of gain compression on picosecond optical pulses in semiconductor optical amplifiers. *J. Mod. Opt.*, vol. 45, pp. 1211-1218, ISSN: 0950-0340.
- Tatham, M. C.; Sherlock, G., & Westbrook, L. D. (1993). Compensation fibre chromatic dispersion by optical phase conjugation in a semiconductor laser amplifier. *Electron. Lett.*, vol. 29, pp. 1851-52, ISSN 0013-5194 Oct. 1993.
- Tomkos, I.; Zacharopoulos, I., Syvridis, D., Calvani, R., Cisternino, F., & Riccardi, E. (1999). All-optical demultiplexing/shifting of 40-Gb/s OTDM optical signal using dual-pump wave mixing in bulk semiconductor optical amplifier. *IEEE Photon. Technol. Lett.*, vol. 11, pp. 1464-1466, ISSN 1041-1135.
- Uchiyama, K.; Kawanishi, S., & Saruwatari, M. (1998). 100-Gb/s multiple-channel output optical OTDM demultiplexing using multichannel four-wave mixing in a semiconductor optical amplifier. *IEEE Photon. Technol. Lett.*, vol. 10, pp. 890-892, ISSN 1041-1135.
- Vahala, K. J.; Zhou, J., Geraghty, D., Lee, R., Newkirk, M., & Miller, B. (1996). Four-wave mixing in semiconductor travelling-wave amplifiers for wavelength conversion in all-optical networks, in T. P. Lee ed. *Current Trends in Optical Amplifiers and Their Applications*. World Scientific, Singapore.
- Xie, C.; Ye, P. & Lin, J. (1999). Four-wave mixing between short optical pulses in semiconductor optical amplifiers with the consideration of fast gain saturation. *IEEE Photon. Technol. Lett.*, vol. 11, pp. 560-562, ISSN 1041-1135.

Yariv, A. (1991). *Optical Electronics*, 4<sup>th</sup> Edition, Saunders College Publishing, San Diego.  
ISBN 0-03-053239-6.

IntechOpen

IntechOpen